INT. J. REMOTE SENSING, 1999, VOL. 20, NO. 1, 97–110

A back-propagation neural network for mineralogical mapping from AVIRIS data

H. YANG†‡, F. VAN DER MEER†, W. BAKKER†
†International Institute for Aerospace Survey and Earth Sciences (ITC), PO Box 6, 7500 AA Enschede, The Netherlands

and Z. J. TAN§
§Peking University, 100871 Beijing, PRC

(*Received 18 March 1997; in final form 13 March 1998*)

Abstract. Imaging spectrometers have the potential to identify surface mineralogy based on the unique absorption features in pixel spectra. A back-propagation neural network (BPN) is introduced to classify Airborne Visible/Infrared Imaging Spectrometer (AVIRIS) of the Cuprite mining district (Nevada) data into mineral maps. The results are compared with the traditional acquired surface mineralogy maps from spectral angle mapping (SAM). There is no misclassification for the training set in the case of BPN; however 17 per cent misclassification occurs in SAM. The validation accuracy of the SAM is 69 per cent, whereas BPN results in 86 per cent accuracy. The calibration accuracy of the BPN is higher than that of the SAM, suggesting that the training process of BPN is better than that of the SAM. The high classification accuracy obtained with the BPN can be explained by: (1) its ability to deal with complex relationships (e.g., 40 dimensions) and (2) the nature of the dataset, the minerals are highly concentrated and they are mostly represented by pure pixels. This paper demonstrates that BPN has superior classification ability when applied to imaging spectrometer data.

1. Introduction

Imaging spectrometers have the potential to identify minerals based on the unique absorption features of their spectra (Ustin and Rock 1985). Imaging spectrometers acquire images simultaneously in many narrow contiguous bands (Goetz *et al.* 1985) which are inherently registered such that each pixel has an associated continuous reflectance spectrum that can be used to identify the surface mineralogy (Vane and Goetz 1985). The 40 bands within 2000–2400 nm wavelength region of Airborne Visible/Infrared Imaging Spectrometer (AVIRIS; Vane *et al.* 1993) 1994 data were used to identify specific minerals or mineral groups through a large number of mineral absorption features for hydroxyl and carbonate minerals (Hunt 1979).

Methods for imaging spectrometer data analysis such as Spectral Angle Mapping (SAM; Yuhas and Goetz 1993, Kruse *et al.* 1993), have been tested to increase the accuracy of the classification results. In this paper we introduce a new approach to

‡e-mail: Yang@itc.nl

International Journal of Remote Sensing
ISSN 0143-1161 print/ISSN 1366-5901 online
http://www.tandf.co.uk/JNLS/res.htm
http://www.taylorandfrancis.com/JNLS/res.htm

imaging spectrometer data analysis using artificial neural networks (ANN), which are brain-like machines that are used in a wide range of applications (Clarkson 1996). We evaluate adopted back-propagation neural network (BPN) for imaging spectrometer data. A comparison is made with the result obtained by spectral angle mapping (SAM) from AVIRIS 1994 data of the Cuprite mining district (U.S.A.). The same training set was used as input for BPN classification and their mean spectra were used for SAM classification. The accuracy of the training set and test set for both BPN and SAM classification was assessed. The results were compared to evaluate the performance of these two classification methods.

2. Approach

2.1. *SAM*

SAM is an automated method for comparing image spectra to a spectral library assuming that the data have been reduced to apparent reflectance (true reflectance multiplied by some unknown gain factor controlled by topography and shadows). The algorithm determines the similarity between two spectra by calculating the 'spectral angle' between them, treating them as vectors in a space with dimensionality equal to the number of bands. In the analysis of images, for each reference spectrum chosen, the spectral angle is determined for each image spectrum (pixel). This value is assigned to the corresponding pixel in the output SAM image, resulting in one output image for each reference spectrum. Grey-level thresholding is used to determine empirically those areas that most closely match the reference spectrum while retaining spatial coherence.

2.2. *BPN*

The ability to learn by example and to generalize, combined with the independence of distribution assumptions make artificial neural networks attractive for supervised classification of remotely sensed data (Schalkoff 1992, Richards 1993, Foody and Arora 1995). The BPN is a new processing system that can examine all the pixels in the image in parallel. It adapts itself to 'learn' the relationship between a set of example patterns and is able to apply the same relationship to new input patterns. This system can focus on the features of an arbitrary input dataset that resembles other patterns seen previously. Furthermore it ignores the noise. The network may be trained to correctly characterize classes in a remotely sensed dataset through an iterative learning process which adjusts the strength of the weights between network units with each iteration (Foody and Arora 1995).

3. Study site

The Cuprite mining district with hydrothermally alteration map shown in figure 1, is situated in southwestern Nevada some 30 km south of the town of Goldfield. It contains both hydrothermally altered and unaltered rocks. The eastern half of the district studied here is an area of extensive hydrothermal alteration within a sequence of rhyolitic welded ash flow and air fall tuffs (Albers and Stewart 1972). These altered rocks can be subdivided into three mappable units: silicified, opalized and argillized rocks. Silicified rocks, containing abundant hydrothermal quartz, form a large irregular patch extending from the middle to the south end of the area. Opalized rocks contain abundant opal and as much as 3 per cent alunite and kaolinite. Locally, an interval of soft, poorly exposed material mapped as argillized rock separates fresh

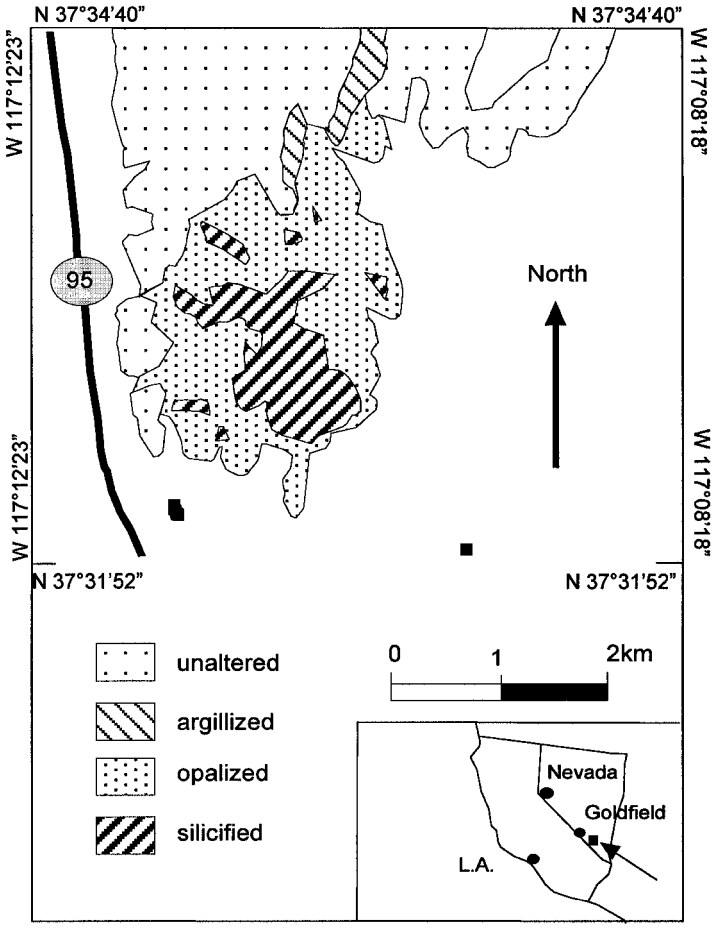

Figure 1. Hydrothermal alteration map of the Cuprite mining district (after Abrams *et al.* 1977).

rocks from opalized rocks. In the argillized rocks, plagioclase is altered to kaolinite, and glass is altered to opal and varying amounts of montmorillonite and kaolinite. The distribution of these alteration assemblages is characteristic for a fossilized hot-spring deposit (e.g., Butchanan 1981) which often contains gold.

The empirical line calibration method was applied to calibrate the radiance data from AVIRIS to reflectance, thus forcing the image data to match selected field reflectance spectra (Roberts *et al.* 1985, Conel *et al.* 1987, Kruse *et al.* 1990). The AVIRIS dataset has been extensively studied by many authors (e.g., Hook *et al.* 1991, Rast *et al.* 1991), and many articles have been published on the use of remote sensing for mineral mapping in the Cuprite mining district by means of other image data analysis techniques (e.g., Kruse *et al.* 1990, Okada and Iwashita 1992, Kahle and Goetz 1983). Because both the geology and the spectral signature of the rocks in this area have been characterized in detail, it is an appropriate dataset for the evaluation of the use of artificial neural networks for imaging data classification and mineralogical mapping.

4. Methods

4.1. *Mineral mapping result of SAM technique*

Select image endmembers: fifteen endmember (as shown in figure 2(*a*)) spectra were selected representing known occurrences of the minerals to be mapped.

Classification: next, the mean spectra (figure 2(*b*)) of the selected endmembers

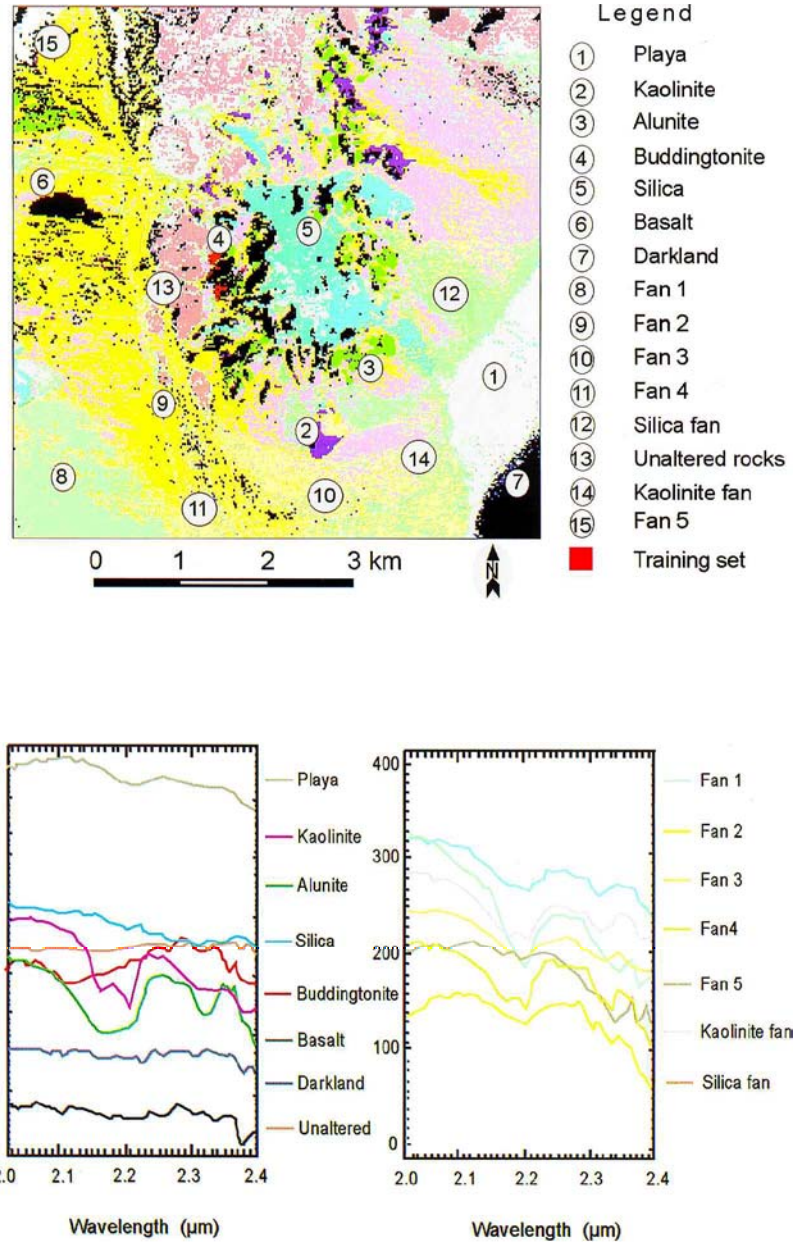

Figure 2. (*a*) Colour composite image of bands 184, 194 and 207 of AVIRIS 1994 as RGB with the training set numbered representing different classes, (*b*) mean spectra of different classes from the training set.

were calculated and used to classify the dataset. The result is a classification image showing the best SAM match at each pixel and a 'rule' image for each endmember showing the actual angular difference in radians between each spectrum in the image and the reference spectrum. Dark pixels in the rule images represent smaller spectral angles, and thus spectra that are more similar to the reference spectrum. The maximum angle thresholding of the 15 classes are: 0.0448, 0.0930, 0.0900, 0.0900, 0.0410, –, 0.0720, 0.0680, 0.0660, 0.1008, 0.0380, 0.0420, 0.0600, 0.0448 and 0.0950 radians, respectively, the same order as in the legend of figure 3 (*a*). SAM produces a class with unclassified pixels. To assist image inspection and to compare with results from BPN, a colour lut is used to discriminate different classes.

4.2. *Classification by the BPN*

4.2.1. *The mechanism of BPN*

A BPN comprises a set of simple processing units arranged in a layered structure with a weighted connection in adjacent layers. Three types of layers may be recognized as shown in figure 4. The input layer comprises one unit for each discriminating variable (e.g., waveband), while the one or more hidden layers each contain a user defined number of units. The output layer contains one unit for each class.

Suppose we have a set of P vector-pairs, (x_1, y_1), (x_2, y_2), …, (x_p, y_p), which are examples of a functional mapping $y = \Phi(x) : x \in R^N, y \in R^N$. We want to train the network so that it will learn an approximation $o = y' = \Phi'(x)$. Learning in a neural network means finding an appropriate set of weights so that we can find the equation of a line that best fits a number of known points. Because the relationship we are trying to map is likely to be nonlinear, as well as multi-dimensional, an iterative version of the simple least-squares method, called steepest-descent technique is applied (Freeman and Skapura 1992). An input vector, $x_p = (x_{p1}, x_{p2}, \ldots, x_{pn})^t$, is applied to the input layer of the network. The input units distribute the values to the hidden-layer units. The net input to the jth hidden unit is

$$net_{pj}^{h} = \sum_{i=1}^{N} w_{ji}^{h} x_{pi} + \theta_j^{h} \tag{1}$$

where w_{ji}^h is the weight on the connection from the ith input unit; N is the total number of the input units; and θ_j^h is the bias term which is the weight on a connection that has its input value always equal to 1. The 'h' superscript refers to quantities on the hidden layer. The output of this node is

$$i_{pj} = f_j^h(net_{pj}^h) \tag{2}$$

Move to the output layer, the net-input values to each unit is

$$net_{pk}^{o} = \sum_{j=1}^{L} w_{kj}^{o} i_{pj} + \theta_k^{o} \tag{3}$$

and the outputs are

$$o_{pk} = f_k^o(net_{pk}^o) \tag{4}$$

where the 'o' superscript refers to quantities on the output layer; The subscript 'p' refers to the pth training vector and 'k' refers to the kth output unit; o_{pk} is the actual output from the kth unit. The error terms for the output units are

$$\delta_{pk}^{o} = (y_{pk} - o_{pk}) f_k^{o\prime}(net_{pk}^o) \tag{5}$$

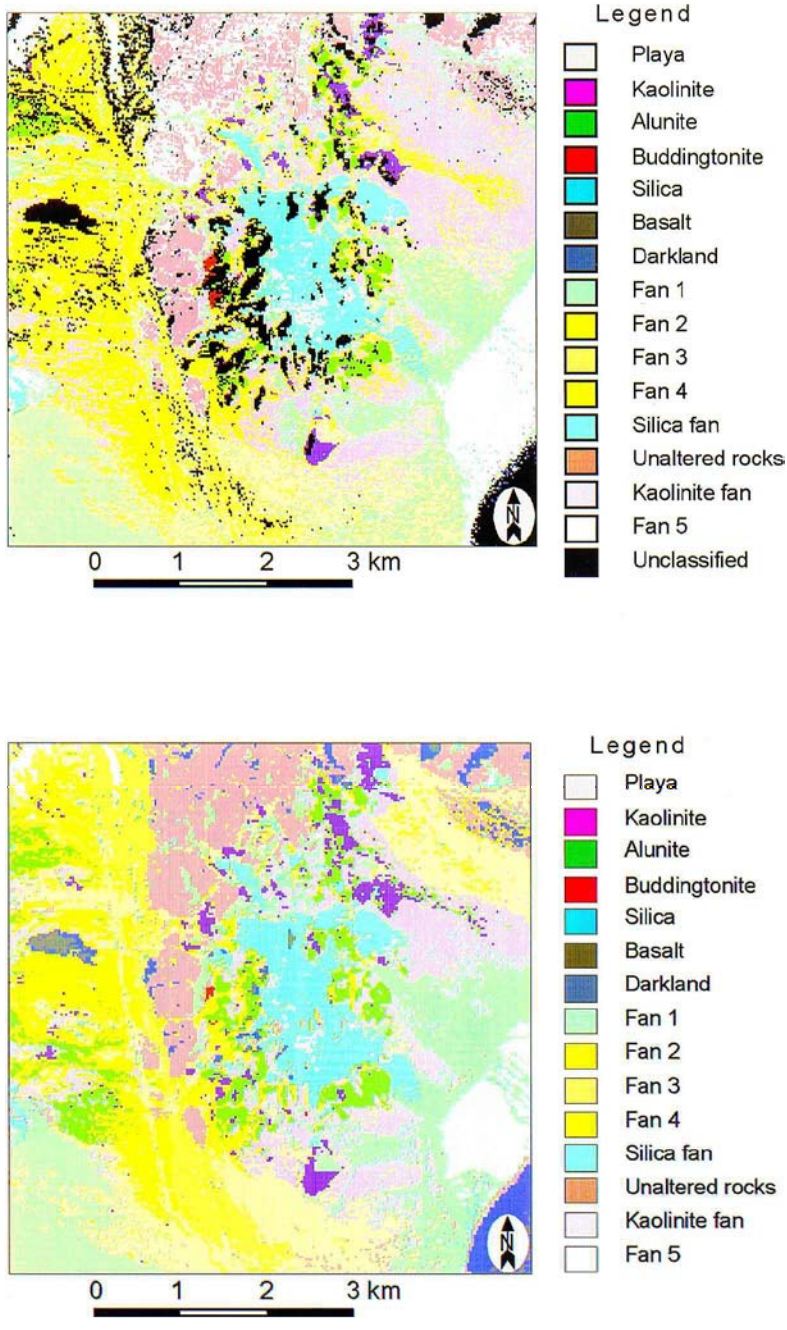

Figure 3. (*a*) Classification results from spectral angle mapper, (*b*) classification results from the back-propagation network.

where y_{pk} is the desired output value and the error terms for the hidden units are

$$\delta^{h}_{pj} = f^{h}_{j}{}'(\mathrm{net}^{h}_{pj}) \sum_{k} \delta^{o}_{pk} i_{pj} \tag{6}$$

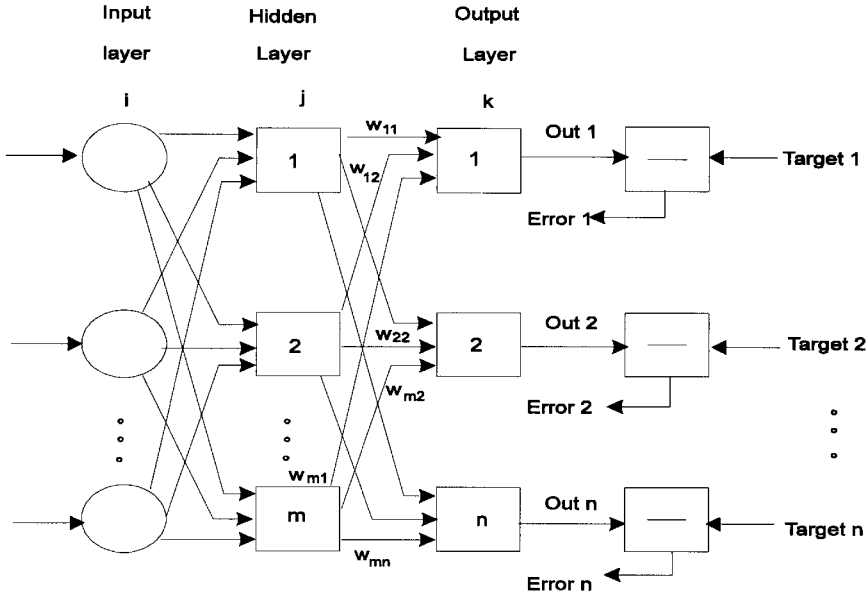

Figure 4. Simplified BPN (after Wasserman 1989).

The error terms on the hidden units are calculated before the connection weights to the output-layer units have been updated. Next the weights are updated on the output layer:

$$w^{o}_{kj}(t+1) = w^{o}_{kj}(t) + \eta\, \delta^{o}_{pk} i_{pj} \tag{7}$$

and update the weights on the hidden layer:

$$w^{h}_{ji}(t+1) = w^{h}_{ji}(t) + \eta\, \delta^{h}_{pj} x_i \tag{8}$$

where the factor η is called learning rate parameter and 't' is the timestep. The order of the weight updates on an individual layer is not important. The error term is

$$E_p = \frac{1}{2} \sum_{k=1}^{M} \delta^{2}_{pk} \tag{9}$$

where 'M' is the total number of output units. Since the quantity is the measure of how well the network is learning, when the error is acceptably small for each of the training-vector pairs (input–output), training can be discontinued.

4.2.2. *Mineral mapping by the BPN network*

4.2.2.1. Neural network structure. Considering the number of bands in the short-wave infrared (SWIR) AVIRIS data (40 bands), a three-single-hidden-layered neural network containing 40 hidden units was created. The network units used a standard sigmoid transfer function with a gain factor of 1. Training each classification involved 800 iterations of a back-propagation learning algorithm with the learning rate and momentum set defined as 0.1 and 0.9, respectively.

4.2.2.2. Training classes and training sample size. The training classes included 15 inputs, the same dataset as used for SAM. Different classes containing different number of pixels with previous knowledge were used. For classes with large spectrally

homogeneous areas, more pixels were selected; for classes with small spectrally homogenous areas, less pixel were selected as shown in figure 2(*a*).

4.2.2.3. Classification. After training is completed, the rest of the image is classified by the acquired network which responds to each new 'unseen' vector with the 'knowledge' gained from the training stage.

The same colour lut used in the SAM results was applied to the BPN classification results (figure 3(*b*)) for comparison.

4.3. *Accuracy assessment*

The classification accuracy was determined in two stages by using contingency tables (error matrices). The cell entries show the number of sampled pixels whose classified category is the column label, and whose true category is the row label ('true' here means having been derived from a presumably more accurate data source than the classification, e.g., ground visit). First, the calibration accuracy was determined. This assessment describes the agreement between the actual class membership for the pixels in the training area and the predicted class membership derived through BPN and SAM classification. These training-area pixels had been used to derive the digital decision rules separating the classes. Second, the validation accuracy was determined by comparing the actual class membership of the test-area pixels to the predicted class membership arrived at by the BPN and SAM classifiers. Test-area pixels are totally independent on the formation of the digital decision rules. About 20 pixels were selected for each class in the training set if possible, which helps to generalize the characteristics of different classes. The test set selected for each class was as large as possible so as to reflect the real situation. The calibration and validation accuracy for the BPN and SAM classification are presented in tables 1–4. Numbers used to represent different classes are the same as in the legend of figure 2 (*a*).

To compare the two classification methods, the overall agreement is computed for each matrix based on the difference between the actual agreement of the classification (e.g., agreement between computer classification and reference data as indicated by the diagonal elements) and change agreement which is indicated by the row and column marginals (Congalton and Mead 1983). This measure of agreement, called KHAT (i.e., $\hat{K}$), is calculated by

$$\hat{K} = \frac{N \sum_{i=1}^{r} x_{ii} - \sum_{i=1}^{r} (x_{+i} * x_{i+})}{N^2 - \sum_{i=1}^{r} (x_{i+} * x_{+i})} \tag{10}$$

where r is the number of rows in the matrix, x_{ii} is the number of the observations in row i and column i, x_{i+} and x_{+i} are the marginal totals of row i and column i, respectively, and N is the total number of observations (Bishop *et al.* 1975).

A KHAT value is computed for each matrix and is a measure of how well the classification agrees with the reference data. Confidence intervals can be calculated for KHAT using the approximate large sample variance (Bishop *et al.* 1975, p. 396)

$$\hat{\sigma}^2(\hat{k}) = \frac{1}{N} \frac{\theta_1(1-\theta_1)}{(1-\theta_2)} + \frac{2(1-\theta_1)(2\theta_1\theta_2 - \theta_3)}{(1-\theta_2)^3} + \frac{(1-\theta_1)^2(\theta_4 - 4\theta_2)^2}{(1-\theta_2)^4} \tag{11}$$

Table 1. Error matrix of the training dataset for ANN classifier in the Cuprite mining district.

	1	2	3	4	5	6	7	8	9	10	11	12	13	14	15	Row total
1	20															20
2		20														20
3			20													20
4				4												4
5					30											30
6						18										30
7							25									18
8								26								26
9									18							18
10										24						24
11											20					20
12												20				20
13													24			24
14														30		30
15															8	8
Column total	20	20	20	4	30	18	25	26	18	24	20	20	24	30	8	307

The producer's accuracy, the user's accuracy and overall accuracy are all 100%.

where

$$\theta_1 = \sum_{i=1} \frac{x_{ii}}{N}, \quad \theta_2 = \sum_{i=1} \frac{x_{i+} * x_{+i}}{N^2},$$

$$\theta_3 = \sum_{i=1} \frac{x_{ii}}{N} \left(\frac{x_{i+}}{N} + \frac{x_{+i}}{N} \right), \quad \theta_4 = \sum_{i=1} \frac{x_{ij}}{N}, \left(\frac{x_{j+}}{N} + \frac{x_{+i}}{N} \right)^2,$$

and x_{j+} is the marginal total of row j.

A test for significance of KHAT can be performed for each matrix separately to determine if the agreement between the classification and the reference data is significantly greater than zero. The test statistic for significant difference in large samples is given by

$$Z = \frac{\hat{k}_1 - \hat{k}_2}{\sqrt{\hat{\sigma}_1^2 + \hat{\sigma}_2^2}} \tag{12}$$

(Cohen 1960). Table 5 shows the KHAT statistic to be used as an accuracy measurement. Notice that with more than 95 per cent confidence, the difference between the BPN and SAM classification is significant. Therefore, based on KHAT values, the BPN classifier is better than the SAM classifier. The result agrees with the overall performance accuracy value given in tables 3 and 4.

5. Discussion

5.1. *Shadows*

The SAM classifier can not handle the classification of shadows and the shadows were all unclassified in SAM. The poor ability to identify the low reflectance features lowered the overall accuracy of the SAM classifier. BPN classifier, on the other

Table 2. The error matrix of the training dataset for SAM classifier in Cuprite mining district.

	1	**2**	**3**	**4**	**5**	**6**	**7**	**8**	**9**	**10**	**11**	**12**	**13**	**14**	**15**	**0***	Row total
1	20				1								2				23
2		20															20
3			16														16
4				4													4
5					29												29
6						0											0
7							4										4
8								26									26
9									18								18
10										21							21
11											19			2			21
12											1	20					21
13													22				22
14														28			28
15															8		8
0*			4			18	21			3						0	46
Column total	20	20	20	4	30	18	25	26	18	24	20	20	24	30	8	0	307

	Producer's accuracy (%)	User's accuracy (%)
1	100	87
2	100	100
3	80	100
4	100	100
5	96.4	100
6	0	—
7	16	100
8	100	100
9	100	100
10	87.5	100
11	95	90.4
12	100	95.2
13	91.6	100
14	93.3	100
15	100	72.7
0*	—	0

Overall accuracy = 255/307 = 83%.

hand, is able to identify some of the minerals in the shadow areas. This might be because the shadows have low reflectance in all bands (dimensions) and SAM classifier only counts the direction but not the magnitude of each spectrum, whereas BPN classifier counts both. The shadows that could not be classified by BPN are not likely to be classified by other classifiers.

5.2. *Pure pixels and mixed pixels*

Among kaolinite, alunite and buddingtonite which are presented mostly in pure pixels, the producer's accuracy of kaolinite and alunite by BPN is much higher than

Table 3. Error matrix of the test set for BPN classifier in Cuprite mining district.

	1	**2**	**3**	**4**	**5**	**6**	**7**	**8**	**9**	**10**	**11**	**12**	**13**	**14**	**15**	Row total
1	156				2											158
2		72	1													73
3		6	68													74
4				4												4
5					136				4		2					142
6						26	113									139
7						9	108									117
8		1						84								85
9									65							65
10									14	25	2		3			44
11									13		100		3	2		118
12					2							143	3			148
13													70			70
14		1	3	1									1	48		54
15															17	17
Column total	156	80	72	5	140	35	221	84	96	25	104	143	80	50	17	1308

	Producer's accuracy (%)	User's accuracy (%)
1	100	98.7
2	90	98.6
3	94.4	91.9
4	80	100
5	97.1	95.7
6	74.3	18.7
7	48.9	92.3
8	100	98.8
9	67.7	100
10	100	56.8
11	96.1	84.7
12	100	96.6
13	87.5	100
14	96	88.9
15	100	100

Overall accuracy = 1122/1308 = 86%.

that of SAM and the producer's accuracy of buddingtonite by BPN is much lower than that of SAM because there were only five pixels used for the test, in which one pixel weights 20 per cent. These results suggest that BPN has higher ability to identify pure pixels than SAM. Varies fans mapped are mostly pixels of mixed minerals. For class 'Fan 1', 'Fan 5' and 'Kaolinite fan', the producer's accuracy of BPN is the same as that of SAM. However, for class 'Fan 3', 'Fan 4' and 'Silica fan', the producer's accuracy of BPN is much higher than that of SAM because there is no or very little misclassification by BPN classifier. Only for class 'Fan 2', the producer's accuracy of BPN is 6.7 per cent less than that of SAM. We may deduce that BPN is also a better classifier than SAM when the pixel is mixed.

Table 4. The error matrix of the test set for SAM classifier in Cuprite mining district.

	1	**2**	**3**	**4**	**5**	**6**	**7**	**8**	**9**	**10**	**11**	**12**	**13**	**14**	**15**	**0***	Row total
1	156				7								12				175
2		52	1														53
3		4	62														66
4				5													5
5					130												130
6						0											0
7							0		2								2
8		2						83									85
9		2	4			1			71		5						83
10						2			15	11							28
11		1			1			1		5	82	23		2			115
12					2				3	1	15	120	6				147
13													60				60
14		1	1										2	48			52
15									1	1	2				17		21
0*		18	4			32	221		4	7						0	286
Column total	156	80	72	5	140	35	221	84	96	25	104	143	80	50	17	0	1308

	Producer's accuracy (%)	User's accuracy (%)
1	100	89.1
2	65	98.1
3	86	93.9
4	100	100
5	93	100
6	0	0
7	0	0
8	99	97.6
9	74	85.5
10	44	39.3
11	79	71.3
12	84	81.6
13	75	100
14	96	92.3
15	100	81
0*	—	0

Overall accuracy = 897/1308 = 69%.

6. Conclusions

There is no misclassification for the training set in BPN; however 17 per cent misclassification occurred in SAM. The calibration accuracy by BPN is higher than that obtained by SAM, suggesting the training process of BPN is better than that of SAM for this dataset. The validation accuracy obtained by SAM is 69 per cent and by BPN 86 per cent, which suggests that both SAM and BPN classifiers have the ability to identify minerals easily separated by their spectra. The high validation accuracy of the BPN has two causes: (1) its ability to deal with complex relationships

Table 5. The result of the test of agreement between error matrices for ANN and SAM classification (with KHAT statistic and its variance).

Z statistic	95% Confidence level
10.44	1.96

Error matrix	KHAT statistic	Variance
ANN	0.8448	0.0001
SAM	0.6639	0.0002

(e.g., 40 dimensions) and (2) the nature of the dataset, the minerals are highly concentrated and they are mostly represented by pure pixels.

Acknowledgment

This research was undertaken with the support of Institute of Remote Sensing Applications, Chinese Academy of Sciences. Special acknowledgments are addressed to Mr Lucas Broekema, Gerrit Huurneman and Wanning Peng for their advice and comments on the study. We also want to thank the two referees for their critical review to improve the quality of the paper.

References

ABRAMS, M. J., ASHLEY, R. P., ROWAN, L. C., GOETZ, A.F.H., and KAYLE, A. B., 1977, Mapping of hydrothermal alteration in the Cuprite mining district, Nevada using aircraft scanner images for the spectral region 0.46–2.36 μm. *Geology*, **5,** 713–718.

ALBERS, J. P., and STEWART, J. H., 1972, Geology and mineral deposits of Esmeralda County, Nevada. *Nevada Bureau Mines Geologic Bulletin*, **78,** 1–80.

BISHOP, Y. M. M., FEINBERG, S. E., and HOLLAND, P. W., 1975, *Discrete Multivariate Analysis—Theory and Practice* (Cambridge, MA: MIT Press).

BUTCHANAN, L. J., 1981, Precious metal deposits associated with volcanic environments in the southwest. In *Relations of Tectonics to Ore Deposits in* the *South Cordillera. Arizona Geology Society Digest*, 24, edited by W. R. Dickinson and W. D. Payne, pp. 237–262.

CLARKSON, T. G., 1996, Introduction to neural networks. *Neural Network World*, **6,** 123–130.

COHEN, J., 1960, A coefficient of agreement for nominal scales. *Educational and Psychological Measurement*, **20,** 37–46.

CONEL, J. E., GREEN, R. O., VANE, G., BRUEGGE, C. J., ALLEY, R. E., and CURTISS, B. J., 1987, Airborne imaging spectrometer-2: radiometric spectral characteristics and comparison of ways to compensate for the atmosphere. In *Proceedings, SPIE*, vol. 834, pp. 140–157.

CONGALTON, R. G., and MEAD, R. A., 1983, A quantitative method to test for consistency and correctness in photointerpretation. *Photogrammetric Engineering and Remote Sensing*, **49,** 69–74.

FOODY, G. M., and ARORA, M. K., 1995, An evaluation of the factors affecting neural network classification accuracy. *Proceedings of the 21st Annual Conference of the Remote Sensing Society, 11-14 September 1995, University of Southampton*, pp. 42–49.

FREEMAN, J. A., and SKAPURA, D. M., 1992, *Neural Networks, Algorithms, Applications, and Programming Techniques* (Addison-Wesley: Reading, MA).

GOETZ, A. F. H., VANE, G., SOLOMON, J. E., and ROCK, B. N., 1985, Imaging spectrometry for earth remote sensing. *Science*, **211,** 1147–1153.

GOETZ, A. F. H., ROCK, B. N., and ROWAN, L. C., 1983, Remote sensing for exploration: an overview. *Economic Geology*, **78,** 573–590.

HOOK, S. J., ELVIDGE, C. D., RAST, M., and WATANABE, H., 1991, An evaluation of short-wave-infrared (SWIR) data from the AVIRIS and GEOSCAN instruments for mineralogical mapping at Cuprite, Nevada. *Geophysics*, **56,** 1432–1440.

HUNT, G. R., 1979, Near-infrared (1.3–2.4 μm) spectra of alteration minerals—potential for use in remote sensing. *Geophysics*, **44,** 1974–1986.

KAHLE, A. B., and GOETZ, A. F. H., 1983, Mineralogical information from a new airborne thermal infrared multispectral scanner. *Science*, **222,** 24–27.

KRUSE, F. A., KEIREIN-YOUNG, K. S., and BOARDMAN, J. W., 1990, Mineral mapping at Cuprite, Nevada with a 63-channel imaging spectrometer. *Photogrammetric Engineering and Remote Sensing*, **56,** 83–92.

KRUSE, F. A., LEFKOF, A. B., BOARDMAN, J. W., HEIDEBRECHT, K. B., SHAPIRO, A. T., BARLOON, J. P., and GOETZ, A. F. H., 1993, The spectral image processing system (SIPS)—Interactive visualization and analysis of imaging spectrometer data. *Remote Sensing of Environment*, **44,** 145–163.

OKADA, K., and IWASHITA, A., 1992, Hyper-spectral image analysis based on waveform characteristics of spectral curve. *Advanced Space Resources*, **12,** 433–442.

RAST, M., HOOK, S. J., ELVIDGE, C. D., and ALLEY, R. E., 1991, An evaluation of techniques for the extraction of mineral absorption features from high spectral resolution remote sensing data. *Photogrammetric Engineering and Remote Sensing*, **57,** 1303–1309.

RICHARDS, J. A., 1993, *Remote Sensing Digital Image Analysis: an Introduction*, 2nd edn (Berlin: Springer-Verlag).

ROBERTS, D. A., YAMAGUCHI, Y., and LYON, R. J. P., 1985, Calibration of Airborne Imaging Spectrometer data to percent reflectance using field measurements. In *Proceedings of Ninth International Symposium on Remote Sensing of Environment, Ann Arbor, MI, October 21–25, 1985.*

SCHALKOFF, R. J., 1992, *Pattern Recognition: Statistical, Structural and Neural Approaches* (New York: Wiley).

TREITZ, P. M., HOWARTH, P. J., SUFFLING, R. C., and SMITH, P., 1992, Application of detailed ground information to vegetation mapping with high spatial resolution digital imagery. *Remote Sensing of Environment*, **42,** 65–82.

USTIN, S., and ROCK, B. N., 1985, Preliminary analysis of AIS spectral data acquired from semi-arid shrub communities in the Owens valley, California. *Proceedings of the Airborne Imaging Spectrometer Data Analysis Workshop, Pasadena, California, April 8–10, 1985*, pp. 41–45.

VANE, G., and GOETZ, A. F. H., 1985, Introduction to the Proceedings of the Airborne Imaging Spectrometer (AIS) Data Analysis Workshop. *Proceedings of the Airborne Imaging Spectrometer Data Analysis Workshop, Pasadena, California, April 8–10, 1985*, pp.21.

VANE, G., GREEN, R. O., CHRIEN, T. G., ENMARK, H. T., HANSEN, E. G., and PORTER, W. M., 1993, Airborne Visible/Infrared Imaging Spectrometer (AVIRIS). *Remote Sensing of Environment*, **44,** 127–143.

WASSERMAN, P. D., 1989, *Neural Computing: Theory and Practice* (New York: Van Nostrand Reinhold).

YUHAS, R. H., and GOETZ, A. F. H., 1993, Comparison of airborne (AVIRIS) and spaceborne (TM) imagery data for discriminating among semi-arid landscape endmembers. *Proceedings of Ninth Thematic Conference on Geologic Remote Sensing, Environmental Research Institute of Michigan, Ann Arbor, MI,* pp. 503–511.